A modification of the ITTC57 correlation line for shallow water

Zeng, Qingsong; Thill, Cornel; Hekkenberg, Robert; Rotteveel, Erik

DOI
10.1007/s00773-018-0578-7

Publication date
2018

Document Version
Final published version

Published in
Journal of Marine Science and Technology (Japan)

Journal of Marine Science and Technology
https://doi.org/10.1007/s00773-018-0578-7

REVIEW ARTICLE

A modification of the ITTC57 correlation line for shallow water

Qingsong Zeng[1] · **Cornel Thill**[1] · **Robert Hekkenberg**[1] · **Erik Rotteveel**[1]

Received: 4 July 2017 / Accepted: 26 June 2018

Abstract
The ITTC57 correlation line, which is derived based on the assumption that the water in which ships advance is infinite deep and wide. However, for ships sailing in the waterway with limited water depth, the frictional resistance will be influenced leading to a decreasing accuracy of the prediction with this correlation line. In this study, a modification of the ITTC57 correlation line is proposed to correct the effects in very shallow water specifically for the flat area of the bottom of the ship. Under some assumptions, this area can be simplified to a 2D flat plate with a parallel wall close to it to study how the shallow water conditions of two interacting boundary conditions are affecting the flat plate friction coefficient. Computational fluid dynamics (CFD) calculations are applied to investigate how a friction line specifically in shallow water deviates from the conventional lines. Such deviations may severely affect the extrapolation of a ship model's resistance to full scale and, therefore, the accuracy of ship's performance prediction. Cases at ten Reynolds numbers from 10^5 to 10^9 are simulated on the 2D flat plate. Seven different distances between the flat plate and the parallel wall were chosen to generate various shallow water conditions, and consequently, a database including frictional resistance coefficients, Reynolds numbers and the distance between those two walls is built. Results indicate that thinner boundary layers are observed in shallow water conditions, and the scale effects which has a significant impact on resistance extrapolation are also observed. Furthermore, the assumption of the zero pressure gradients (ZPG) which is commonly used in deep water is no longer valid in extremely shallow ones. Finally, a modification for the ITTC57 correlations line considering shallow water effects is proposed, which is willing to improve the prediction of the frictional resistance of those ships with a large area of flat bottom and sail in shallow water.

Keywords Shallow water · Friction line · CFD · Boundary layer · Zero pressure gradient

List of symbols

C_f	Total friction resistance coefficient
C_{fx}	Local friction resistance coefficient
d	Distance between the sample point and the flat plate (m)
CFD	Computational fluid dynamics
D	Distance between flat plate and parallel wall (m)
D_n	The distance between the parallel wall and the flat plate at the case n (m)
EFD	Experimental fluid dynamics
h	Water depth
h_i	A parameter which identifies the grid cell size
I	The turbulence intensity
L	Length of flat plate (m)
N	Number of nodes
p	Pressure (Pa) and dimensionless pressure
R	A symbol representing errors in grid study
Re	Total Reynolds number
Re_x	Local Reynolds number
Re_θ	Momentum boundary layer thickness Reynolds number
$Re_{\_0}$	Reynolds number of the incoming flow
$Re_{\_B}$	Reynolds number of the flow underneath ship's bottom
S_B	Wetted surface of the flat bottom of a ship or model
S_T	Wetted surface of a ship or model
T	The draft of the ship of model
t	Time (s) and dimensionless time
u_x	Velocity (m/s) and dimensionless velocity in horizontal direction
u_y	Velocity (m/s) and dimensionless velocity in vertical direction
U^+	A dimensionless velocity
U_∞	Flow velocity (m/s)
U_{ave}	The Reynolds averaged velocity

✉ Qingsong Zeng
Q.Zeng@tudelft.nl

[1] Delft University of Technology, 2628CD Delft, The Netherlands

Published online: 11 July 2018

$V_{\_0}$	The velocity of the incoming flow
$V_{\_B}$	The average input velocity of the flow underneath ship's bottom
y^+	y plus, a non-dimensional wall distance for a wall-bounded flow
κ	Von Kármán constant
μ	The molecular dynamic viscosity
μ_t	The turbulent viscosity
ν	Kinematic viscosity (m^2/s)
τ_w	Wall shear stress

1 Introduction

An improved understanding of the characteristics of friction/correlation lines in various conditions can contribute a better model-ship extrapolation, which is in turn beneficial for ship design and optimization. Such prediction is based on the understanding of the boundary layer theory and friction lines derived from a flat plate. In the past century, researchers have provided several friction lines, e.g. Schoenherr [1], Grigson [2] and Katsui [3] proposed friction lines for flat plates and 1957 ITTC [4] correlation line is frequently used to predict the frictional resistance of ships. These methods were based on the results of experiments and/or numerical simulations with an unrestricted incoming flow. In these cases, the pressure gradient along the flat plate is assumed to be zero.

However, practically, the incoming flow is usually restricted. For inland ships which sail in rivers and canals, ship resistance is influenced by waterway limitations. The 1987 ITTC [5] indicated that shallow water effects will be noticeable when the ratio of water depth to ship draft is less than 4.0. Various researchers [6–8] provided ways to predict the resistance in shallow water but without specifically and physically discussing the changes of friction, which is the major part of the resistance of most inland vessels. As the effects from the lateral direction (i.e. the effects of the sides of the waterway) are much smaller than the vertical direction (i.e. the waterway bottom) [9], this study will focus on the effects on the flat plate friction in pure shallow water only. Additionally, the inflow conditions into the slit between ship's and fairway's bottom are subject to form- and flow pattern effects (towards more 2D patterns in very shallow waters), and these effects are subject to ongoing investigations.

For waterways with unlimited width, shallow water mainly affects the bottom area of the ship, and the effects on other wetted surfaces can be ignored. Since the ITTC57 correlation line cannot resolve shallow water effects, especially for the extremely shallow water [10], this correlation line should be corrected for shallow water effects.

Generally, most inland ships have a long parallel midbody and a large area of the flat bottom. The characteristics of the flow close to the bottom are comparable with the flow passing above a 2D flat plate, as shown in Fig. 1 (this is further illustrated in Sect. 2.1). We assume the velocity of far-field incoming water is V (ship-based coordinate system), and the water underneath the ship is accelerated by ΔV (due to the displacement of the ship and/or the limitation of the waterway). This acceleration even happens in deep water but will be more obvious in shallow water. Therefore, in the simplification, the speed of incoming water for the flat plate should be $V+\Delta V$. For illustrating convenience, we keep using the symbol V to represent the velocity for flat plate and revert to the $V+\Delta V$ when calculating ship's friction; similarly, we also keep using the symbol L for the length of the plate.

A 2D flat plate has been seen as a reasonable simplification for investigating the physics of friction [2, 3]. In the research of Eça and Hoekstra [11], systematic calculations of frictional resistance using CFD have been done on a flat plate with a plenty number of turbulence models. In their research, the parallel boundary was deliberately set far enough away from the flat plate to avoid shallow water effects. They compared the results when the distances between the flat plate and the parallel boundary were $0.25L$ and $0.5L$, where L is the length of the plate, and concluded that the differences were too small to be considered. However, a distance less than $0.25L$ is quite common in practice, e.g. for some ports and inland waterways, the under-keel clearance may be even smaller than $0.01L$ [12].

In this study, extremely small under-keel clearances (up to $0.01L$) are included. Shallow water effects on the physical details of boundary thickness and pressure gradients are investigated. CFD techniques are applied and it is found that both the pressure gradients along the plate and the friction were affected by the flow limitation. Finally, a regression

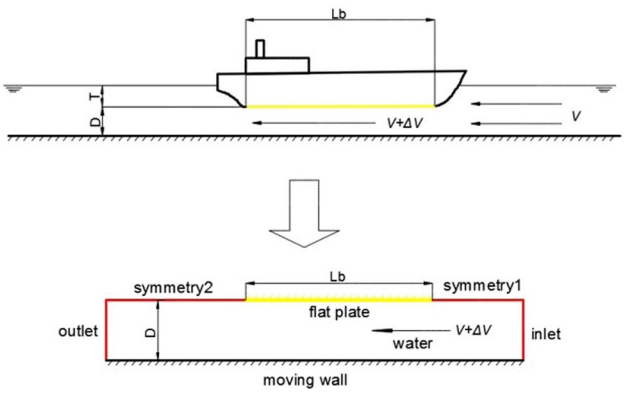

Fig. 1 Simplification of ship bottom in shallow water (ship-based coordinate system; L_b is the length of the flat bottom, D the under keel clearance, T the draft, V and $V+\Delta V$ are the initial and accelerated velocities)

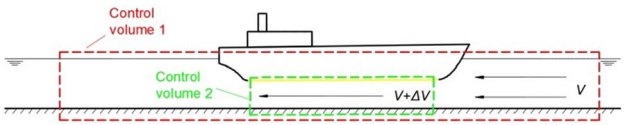

Fig. 2 The chosen of the control volume

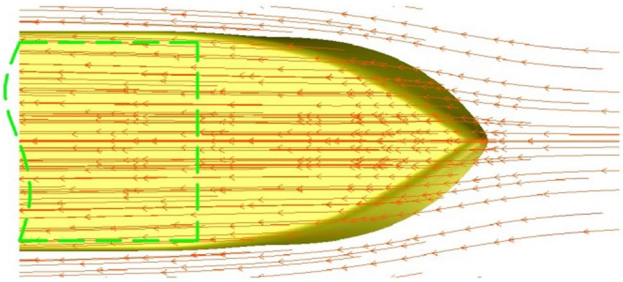

Fig. 3 An example of water path lines underneath an inland vessel (1/30 model, $h/T=1.5$, $V=0.8$ m/s, $L=2.86$ m, $T=0.117$ m, the green rectangle indicates the selected area)

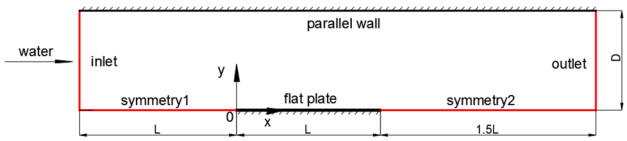

Fig. 4 Computational domain

Table 1 The seven computational cases (D_n means the distance between the parallel wall and the flat plate at the case n)

Case	D/L	D_{n+1}/D_n
1	1.00	0.32
2	0.32	0.5
3	0.16	0.5
4	0.08	0.5
5	0.04	0.5
6	0.02	0.5
7	0.01	–

analysis is made based on the CFD results to propose a numerical friction line for the flat plate in shallow water. Practically, to improve the prediction of ship's friction, after applying ITTC57 correlation line for all wetted surface, this proposed line can be used to correct the shallow water effects on a ship's flat bottom. The combination of these two lines is considered as a suitable method for predicting the frictional resistance in the pure shallow water.

This paper consists of five sections. Section 2 introduces the computational setup and the selection of boundary conditions. Section 3 provides the verification and validation by analyzing the numerical uncertainty and modeling errors. Section 4 presents the results of CFD simulations and the fitting of the numerical friction line; an example of how to apply the method is given. Conclusions are drawn in Sect. 5.

2 Approach

The feasibility of the 2D flat plate simplification is first discussed in this section. The shallow water conditions were obtained by adjusting the distance between the flat plate and a parallel wall. In this study, calculations were performed in a RANS solver: ANSYS$^{(TM)}$ Fluent (version 16.2). The Reynolds number in the simulations was varied from 10^5 to 10^9.

2.1 Simplification

In practice, reasonable simplification can help to understand the nature of a phenomenon but with much smaller resources. In this study, we assume the flow passing above a 2D flat plate can represent the flow close to the flat bottom of inland vessels.

Physically, due to the presence of the bow and the stern, part of the water around a ship flows laterally leading to the dissatisfaction of the continuity of fluid on the longitudinal center plane. However, if we change the control volume from 1 to 2, as shown in Fig. 2, the continuity equation can be satisfied.

To further illustrate the assumption, an example is done for an inland vessel. As depicted in Fig. 3, part of the water flows away from the longitudinal center plane at the bow. These effects shall be considered by appropriate corrections imposed to the inflow boundary conditions for the 2D investigated flat bottom plate. Through this, when the water goes into the space underneath the bottom of the ship, its direction is no longer changed and the characteristics of the flow are comparable to that above a 2D flat plate.

Therefore, for the control volume 2, it is rational to apply the simplification mentioned at the beginning of this section.

2.2 Computational model

The computational domain is shown in Fig. 4. For conventional viewing angle, the domain is rotated by 180° compared with that in Fig. 1.

The flat plate used in this study is two meters long (L), and the domain stretches L in front of the plate and $1.5L$ behind it. A geometric progression with a factor of 0.5 is implemented for the distances (D) between the parallel wall and the plate, as depicted in Table 1.

Case 1 simulates the deep water condition for comparison. Case 7 is considered to be extremely shallow water. For example, $D/L=0.01$ means a ship with 100 meters

long flat bottom sails in a shallow waterway with the under-keel clearance of only 1 m.

The flow is the fresh water with a density of 999.04 kg/m^3 and a kinematic viscosity of1.13902×10^{-6}m/s^2. This study used ten Reynolds numbers in the range from 10^5 to 10^9, as shown in Table 2.

Four turbulence models were chosen to simulate the characteristics of the flow: Three fully-turbulent models (Spalart–Allmaras (SA), BSL k-ω and SST k-ω) and one transition model (k-kl-ω).

2.3 Mesh generation

The number of grid points in the *x*-direction is identical for most cases (mesh was refined for the shallowest cases and part of the high *Re* cases), and the distribution of grid points close to the flat plate is similar for all cases. The number of grid points in the *y*-direction decreases with the decrease of the distance (*D*). Additionally, the mesh close to the flat plate and that close to the parallel wall was refined from case 2 to case 7, because shear stress was observed on these boundaries.

Denser grids were generated near the flat plate as well as the area close to plate's leading and trailing edge, as shown in Fig. 5 (The number of grid cells in the picture has been reduced for illustration). Grids were also refined close to the moving wall for all cases except for the cases with $D/L = 1.00$ because the shear stress on the moving wall when $D/L = 1.00$ is too small to be considered. The "BiGeometric" bunching law [13] was applied to the nodes distribution, indicating that the space expansion between the nodes in each direction is linear.

Table 2 Investigated Reynolds numbers

No.	*V* (m/s)	*Re*	lg (*Re*)
1	0.2267	3.9811×10^5	5.6
2	0.5695	1.0000×10^6	6.0
3	1.4305	2.5119×10^6	6.4
4	3.5934	6.3096×10^6	6.8
5	9.0261	1.5849×10^7	7.2
6	22.6726	3.9811×10^7	7.6
7	56.9510	1.0000×10^8	8.0
8	143.0544	2.5119×10^8	8.4
9	359.3365	6.3096×10^8	8.8
10	902.6125	1.5849×10^9	9.2

2.4 Boundary conditions

2.4.1 Inlet boundary

An incompressible, undisturbed flow enters the domain from the inlet with a velocity of U_∞. The inlet boundary applies Dirichlet conditions for both velocity and turbulence quantities:

$$u_x = U_\infty,\ u_y = 0;$$

$$I \equiv \frac{u'}{U_{\text{ave}}} = C_1, \frac{\mu_t}{\mu} = C_2. \tag{1}$$

In Eq. 1, u_x and u_y are the velocities of upstream flow in *x* and *y* direction, respectively. *I* is the turbulence intensity, u' the root-mean-square of the turbulent velocity fluctuations, U_{ave} the Reynolds averaged velocity, μ_t the turbulent viscosity, and μ the molecular dynamic viscosity. C_1 and C_2 are both constants, which will be chosen in this section.

The static pressure at the inlet boundary is set to zero. The total pressure is not a constant value but will rise to whatever value is necessary to provide the prescribed velocity distribution [14].

In the research of Walters [15], where the three-equation transition model (k-kl-ω) was proposed, three different inlet boundary conditions were applied. Similar sets were chosen in this study (see Table 3).

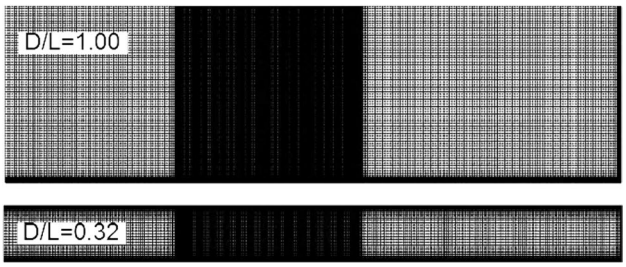

Fig. 5 Mesh generation

Table 3 The alternative inlet boundary conditions

Set	*I* (%)	μ_t/μ
1	0.9	9
2	0.9	12
3	0.9	100
4	3	9
5	3	12
6	3	100
7	6	9
8	6	12
9	6	100

The friction on the flat plate was recorded and shown in percent compared to a randomly chosen set (Set5: $I=3\%$, $\mu_t/\mu=12$), which is listed in Table 4. For the SA model in Fluent, the alteration of turbulence intensity is not available when different is set. Thus, the results of friction were compared to $\mu_t/\mu=12$ without setting a specific intensity. Comparisons are made for two Reynolds numbers: one is relatively low ($Re=2.51\times10^6$) for which the transition from laminar flow to turbulent flow is obvious; another one is high ($Re=1.58\times10^9$) for which the turbulent flow is dominant.

Based on Table 4, we found

- For the high Reynolds number, the friction is insensitive to different I and μ_t/μ; even the maximum difference is less than 0.1%;
- For the relatively low Reynolds number ($Re=2.51\times10^6$), the calculations with the BSL k-ω and the SST k-ω model also show insensitivity to inlet boundary conditions (maximum 1.2%). For those with the SA model, the deviation is larger but still less than 5%. However, for the k-kl-ω model, the results show big discrepancies especially when $\mu_t/\mu=100$, because different inlet boundary conditions significantly affect the position of "transition point" from laminar flow to turbulent flow, and the k-kl-ω model can more successively catch these changes;
- For the calculations with fully turbulence models, higher turbulent viscosity ratio (μ_t/μ) leads to larger friction.

Consequently, for the BSL k-ω and SST k-ω models, the turbulence intensity and turbulent viscosity ratio at the inlet boundary have minor impacts on results. For the SA model, the influence of boundary conditions is noticeable, and for the k-kl-ω model, the results significantly depend on the boundary conditions. Which model is the most suitable one is decided after verification and validation (see Sect. 3).

2.4.2 Other boundary conditions

The "pressure outlet" was set at the outlet boundary. All derivatives of the flow quantities at x direction were set to zero. The position of outlet boundary should be far enough from the flat plate to avoid influencing the gradient of fluid variables in the domain. Figure 6 shows the pressure gradient at x direction from the trailing edge to the outlet. Three distances (0.5L, 1.0L and 1.5L, $L=2$ m) are tested.

For the outlet boundary of 0.5L, 1.0L and 1.5L behind the flat plate, the pressure gradients to the x-direction near the outlet boundary are 1.149, 0.186 and 0.0074, respectively. A value close to zero means the outlet boundary is far enough and will not affect the flow. Therefore, the outlet boundary which is 1.5L behind the plate is enough for this study.

In addition, for the "backflow" (if any) at outlet boundary, Dirichlet conditions were set to the turbulence intensity and turbulence-viscosity ratio with the same values as at the inlet boundary.

The parallel wall was set as a non-slip "moving wall" with the same speed as the free stream. All derivatives of the flow

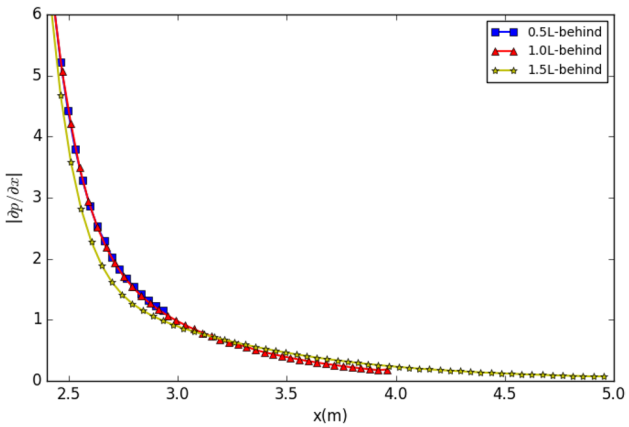

Fig. 6 Pressure gradient at x direction from the trailing edge to the outlet boundary

Table 4 Influence of inlet boundary conditions on friction (compare to Set 5, shown in percent, %)

Turbulence model	I %	μ_t/μ ($Re=2.51\times10^6$)			μ_t/μ ($Re=1.58\times10^9$)		
		9	12	100	9	12	100
SA	–	−0.37	0.00	4.60	0.00	0.00	0.02
BSL k-ω	0.9	−0.05	0.00	0.37	0.00	0.01	0.08
	3	−0.07	0.00	1.10	−0.01	0.00	0.05
	6	−0.07	−0.02	1.19	−0.01	−0.01	0.03
SST k-ω	0.9	−0.04	−0.01	0.19	0.01	0.02	0.09
	3	−0.04	0.00	0.72	0.00	0.00	0.06
	6	−0.05	−0.01	0.79	−0.01	0.00	0.04
k-kl-ω	0.9	0.05	−0.29	−13.14	–	–	–
	3	0.24	0.00	87.91	–	–	–
	6	0.07	0.16	92.95	–	–	–

quantities in the y-direction were set to zero, and the speed relative to the parallel wall in the x-direction was set to zero.

The flat plate was set as a still, non-slip wall. Dirichlet conditions were set to the velocities, i.e. velocities at x and y directions were zero.

Symmetry conditions were set in front and behind the flat plate. The velocity and the derivatives of all flow quantities at the y-direction were set to zero.

3 Verification and validation

Numerical simulations shall be verified and validated before application. This is done in Sect. 3.1 and 3.2 respectively.

3.1 Verification

The verification gives the numerical error and uncertainty of a simulation. Typically, a numerical error is the discrepancy between a numerical result and the exact solution. According to Roache [16], the numerical error contains three components: round-off error, iterative error, and discretization error.

Round-off error results from the finite precision of the computers, but the double precision format can usually keep this error negligible [17]. The iterative error is a consequence of the non-linearity of the mathematical equations. Using double-precision scheme and a sufficient number of iterations can normally reduce this error to the level of the round-off error. In this study, the convergence criteria of all residuals are set to 10^{-7}. This does not mean the iterative error is 10^{-7}, and actually, this usually keeps the iterative error at the level of 10^{-9}. The discretization error is generated when transforming the partial differential equations into algebraic equations and mostly dominates the numerical error. Therefore, in this article, only the discretization error is considered.

A grid refinement study is commonly used to estimate the discretization error [16]. At least four grids are recommended [18] to justify whether the results are in the "asymptotic region". In this verification, four geometrically similar grids (G1–G4) with a refinement ratio of 1.6 were generated for the Case1 ($D/L = 1.0$, the deep case). Both the number of nodes (Table 5) and the distance between the nodes (e.g. the y^+, see Table 6) had a ratio as close as possible to 1.6. No wall functions were used, and even the coarsest grid had a y^+ less than 1.

In this grid refinement study, a turbulence intensity of 3% and a turbulent viscosity ratio of 12 were used. Two Reynolds numbers ($Re = 2.51 \times 10^6$ and $Re = 1.58 \times 10^9$) were chosen for the verification with three turbulence models, as shown in Fig. 7.

The scale of different grids can be represented by a symbol h_i, which is defined as follows:

$$\frac{h_i}{h_1} = 1.6^i = \frac{N_{x1}}{N_{xi}} = \frac{N_{y1}}{N_{yi}},$$

where h_i is the symbol representing the scale of Grid i; N_{xi} and N_{yi} are the numbers of Grid i at x and y directions, respectively. The value of h_1 is set to 1 by default. The value of h_i is useful for presenting the results of grid refinement study (i.e. the x-axis of Fig. 7).

Although this study applied the three-equation k-kl-ω model for $Re = 2.51 \times 10^6$, the results showed oscillatory convergence (Table 7).

The symbol R is defined as

$$R = \frac{C_{f_i} - C_{f_{i-1}}}{C_{f_{i-1}} - C_{f_{i-2}}}.$$

where C_{fi} is the frictional resistance coefficient of Grid i ($i \geq 3$). For $R < 0$ and $|R| < 1$, C_{f} has an oscillatory convergence [18].

Following the procedure of numerical uncertainty analysis proposed by Eça and Hoekstra [18], the uncertainty of C_{f} for the finest grid (G1) and the corresponding observed order of accuracy p is shown in Table 8. Since only the monotonously convergence was considered, the uncertainty analysis of the calculations with the k-kl-ω model was excluded in this table.

Based on Fig. 5 and Table 8, it can be observed

Table 5 Number of nodes in x and y directions for two Reynolds numbers in Case 1 ($D/L = 1.0$)

lg (Re)		G1	G2	G3	G4
All	N_x	755	471	295	183
6.4	N_y	269	169	105	65
9.2	N_y	377	237	149	93

Table 6 Values of y^+ of the first layer of grid above the plate

No.	lg(Re)	G1	G2	G3	G4
1	5.6	0.200	0.320	0.512	0.820
2	6.0	0.200	0.319	0.511	0.817
3	6.4	0.200	0.320	0.512	0.820
4	6.8	0.202	0.323	0.517	0.828
5	7.2	0.205	0.328	0.525	0.840
6	7.6	0.207	0.331	0.530	0.848
7	8.0	0.212	0.339	0.542	0.867
8	8.4	0.212	0.340	0.544	0.870
9	8.8	0.214	0.342	0.547	0.876
10	9.2	0.211	0.337	0.540	0.863

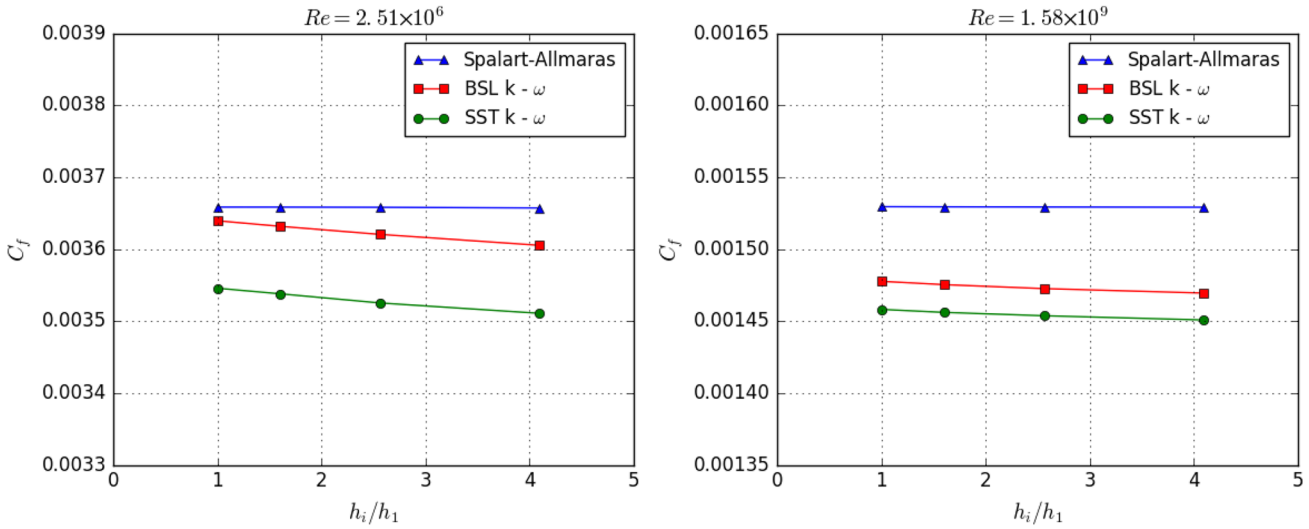

Fig. 7 Frictional resistance coefficient C_f with the refinement of grids

Table 7 Grid refinement study with k-kl-ω model for $Re = 2.51\times10^6$

Grid	C_f ($\times10^{-3}$)	R
G1	1.5166	−0.830
G2	1.5602	−0.676
G3	1.5077	−0.049
G4	1.5854	–

Table 8 The observed order of accuracy and uncertainty of C_f for the finest grid (G1)

Turbulence model	$Re = 2.51\times10^6$		$Re = 1.58\times10^9$	
	p	Uncertainty	p	Uncertainty
SA	2.49	0.042%	1.00	0.047%
BSL k-ω	0.57	0.919%	0.71	0.376%
SST k-ω	0.61	0.867%	0.74	0.326%

- In the grid refinement study, the value of C_f depends on Reynolds number and the selected turbulence models. C_f increases with the refinement of the mesh. Calculations with SA model generate the highest C_f and SST k-ω leads to the lowest C_f for both Reynolds numbers;
- The chosen turbulence models affect the C_f more than the density of grids. Those changes of C_f become smaller with the mesh refinement;
- Calculations at $Re = 1.58\times10^9$ show smaller uncertainty than that at $Re = 2.51\times10^6$, but both of their uncertainties are smaller than 1%.

Consequently, the finest grid (Grid 1), which has been verified in this section, was chosen for the further systematic simulations.

3.2 Validation

After estimating the numerical uncertainty, the deviations of simulations from experimental data (modeling error) are estimated.

In this section, the results of global friction (C_f) on the flat plate are validated using the friction lines proposed by Prandtl—Schlichting [19] and Katsui et al. [3]. Different inlet boundary conditions listed in Table 3 are compared and the best suitable one is chosen in Table 9. Finally, the local skin friction and the mean flow velocity profile, are validated with the experimental data of Nagib et al. [20].

Formulas of Prandtl–Schlichting and Katsui friction lines are as follows:

1. The Prandtl–Schlichting line [19]:

$$C_f = \frac{0.455}{(lgRe)^{2.58}}$$

2. The friction proposed by Katsui et al. [3]:

$$C_f = \frac{0.0066577}{(\lg Re - 4.3762)^a}$$

$$\text{for}: 1\times10^6 \le Re \le 7\times10^9$$

$$\text{where}: a = 0.042612\lg Re + 0.56725.$$

For both $Re = 2.51\times10^6$ and $Re = 1.58\times10^9$, the difference of C_f in unrestricted condition ($D/L = 1.0$) is compared with these two friction lines, which is shown in Table 9.

From Table 9, it can be derived that

Table 9 Differences of C_f compared with methods of Prandtl–Schlichting and Katsui et al. at both $Re = 2.51 \times 10^6$ and $Re = 1.58 \times 10^9$(shown in percent, %)

Turbulence model	I (%)	Compared with Prandtl–Schlichting method						Compared with Katsui method					
		$Re = 2.51 \times 10^6$ μ_t/μ			$Re = 1.58 \times 10^9$ μ_t/μ			$Re = 2.51 \times 10^6$ μ_t/μ			$Re = 1.58 \times 10^9$ μ_t/μ		
		9	12	100	9	12	100	9	12	100	9	12	100
SA	–	−3.70	−3.34	1.11	3.07	3.07	3.10	−1.02	−0.65	3.92	3.95	3.95	3.97
BSL k-w	0.9	−3.89	−3.85	−3.48	−0.41	−0.40	−0.33	−1.21	−1.17	−0.80	0.43	0.44	0.52
	3	−3.89	−3.84	−2.78	−0.42	−0.41	−0.36	−1.22	−1.17	−0.08	0.43	0.43	0.48
	6	−3.91	−3.86	−2.70	−0.42	−0.42	−0.38	−1.24	−1.19	0.00	0.43	0.43	0.47
SST k-w	0.9	−6.34	−6.32	−6.13	−1.72	−1.71	−1.64	−3.74	−3.71	−3.52	−0.88	−0.88	−0.80
	3	−6.34	−6.31	−5.63	−1.73	−1.73	−1.67	−3.74	−3.70	−3.01	−0.89	−0.89	−0.83
	6	−6.35	−6.32	−5.57	−1.74	−1.73	−1.69	−3.75	−3.72	−2.94	−0.90	−0.89	−0.85
k-kl-w	0.9	−59.91	−60.05	−65.20	–	–	–	−58.80	−58.94	−64.23	–	–	–
	3	−59.84	−59.93	−24.71	–	–	–	−58.72	−58.82	−22.61	–	–	–
	6	−59.90	−59.87	−22.69	–	–	–	−58.79	−58.75	−20.54	–	–	–

- The simulations with SA model overestimate the C_f by 1–4% for$\mu_t/\mu = 100$ at $Re = 2.51 \times 10^6$ and for all conditions at $\mathrm{Re} = 1.58 \times 10^9$;
- Simulations with BSL and SST k-w model agree will the two friction lines; and the results with BSL k-ω model agree better, especially when $I = 6\%$ and $\mu_t/\mu = 100$;
- The results with the k-kl-ω model show smaller values because this model catches larger laminar regions than fully turbulence models.

For full-scale ships, turbulent boundary layer starts immediately after the flow reaches the bow and dominates the whole boundary layer. Therefore, a similar proportion of turbulent boundary layer is expected for the geometrically similar model ships. To achieve this, turbulence stimulations (such as sand, tripwire, and pins [21]) are applied. Consequently, using fully turbulence models is more comparable with the physics of ship model tests than using a transition model. Additionally, according to Table 9, the BSL k-ω model with $I = 6\%$ and $\mu_t/\mu = 100$ has a good agreement with the fully turbulent method at both low and high Reynolds numbers. This set of turbulence model and boundary conditions are, therefore, chosen for further systematic simulations.

Nagib et al. [20] evaluated many previously proposed empirical local friction formulas based on the more recent experimental datasets (Nagib et al. [22] and Österlund [23]). Through proper modifications, they concluded that those formulas can accurately describe the local friction. The mean velocity profiles in the turbulent boundary layers were also shown in a graph against a large range of momentum thickness Reynolds number (Re_θ), which provides validating data for this research.

Based on the fitting of Nagib, the local Reynolds number (Re_x) can be converted to the momentum thickness Reynolds number (Re_θ) using

$$Re_\theta = 0.01277(Re_x)^{0.8659}.$$

The CFD calculations of local friction coefficients (C_{fx}) are validated in Fig. 8. Compared the fitting results of Nagib, the CFD calculations have up to 6% higher values for C_{fx}. If the classical local friction line, i.e. Prandtl–Schiliching, is used, the CFD results generally underestimate the C_{fx} by about 4%. The data of Nagib is based on more recent experiments, which are assumed to be more reliable. Nevertheless, an error less than 6% is practically acceptable for CFD calculations unless an extremely rigorous requirement is posed.

Additionally, the mean velocity profiles are validated in Fig. 9. The CFD results agree well with the experiments,

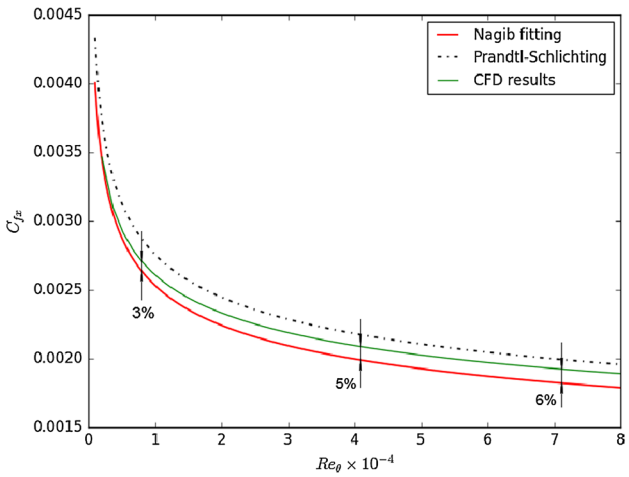

Fig. 8 The local friction coefficient is shown against Re_θ (the friction line of Prandtl–Schlichting is shown)

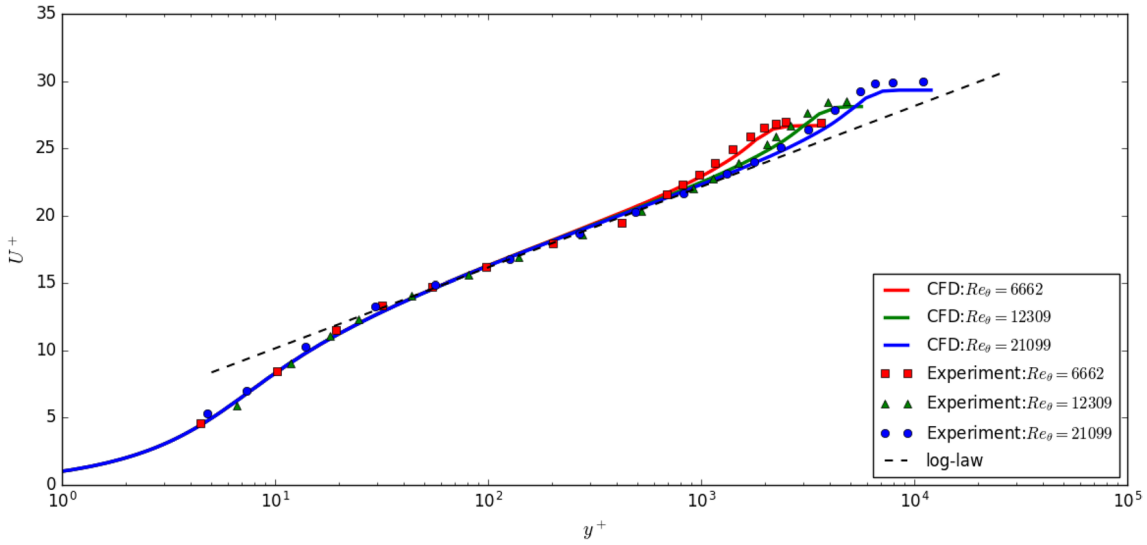

Fig. 9 Mean velocity profiles and log-law diagnostic function against y^+ (U^+ is the dimensionless velocity defined by $U^+ = u/\sqrt{\tau_w/\rho}$, where u is the flow velocity parallel to the plate and τ_w is the wall shear stress; in the logarithmic law, $\kappa = 0.394$ according to Nagib)

especially for the viscous sublayer ($y^+ < 8$, roughly) and log-law region ($50 < y^+ < 500$, roughly). In other regions, CFD calculations tend to underestimate the velocity, which means a thinner boundary layer and thus a higher velocity gradient, which can also explain the discrepancies of the C_{fx} in Fig. 8.

Based on the validation, CFD techniques applied in this study have acceptable errors and can be trusted for further calculations.

4 Results and analysis

The systematic simulations involve ten Reynolds numbers and seven shallow water conditions, as shown in Table 10. The number of grid cells in the x-direction (Nx) is unchanged from $Re = 3.9811 \times 10^5$ to $Re = 2.5119 \times 10^8$, and to stabilize the calculation, Nx was increased to 827 (finer mesh) at higher Reynolds numbers. The number of grid cells in the y-direction (Ny) was varied according to the distance between the flat plate and the parallel wall.

4.1 The physical effects of shallow water on friction

Physically, the flow will be accelerated due to the displacement of the boundary layer, leading to a thinner boundary layer especially in extremely shallow water conditions. To clarify the changes of boundary layers, a square area close to the flat plate was chosen, as shown in Fig. 10. The boundary layer thicknesses at the trailing edge of the plate at two Reynolds numbers are shown in Fig. 11. The space in the y-direction is amplified 5 times to clearly illustrate the physical details in the boundary layer.

From Fig. 11, some remarks can be derived:

Table 10 Number of nodes in x and y directions at different conditions

No.	*Re*	lg(*Re*)	*Nx*	*D*/*L* = 1.00 *Ny*	*D*/*L* = 0.32 *Ny*	*D*/*L* = 0.16 *Ny*	*D*/*L* = 0.08 *Ny*	*D*/*L* = 0.04 *Ny*	*D*/*L* = 0.02 *Ny*	*D*/*L* = 0.01 *Ny*
1	3.9811×10^5	5.6	755	237	165	113	85	65	45	29
2	1.0000×10^6	6.0	755	253	177	125	97	77	57	41
3	2.5119×10^6	6.4	755	269	189	137	109	89	69	53
4	6.3096×10^6	6.8	755	285	201	149	121	101	81	65
5	1.5849×10^7	7.2	755	301	213	161	133	117	93	77
6	3.9811×10^7	7.6	755	313	225	173	145	129	105	89
7	1.0000×10^8	8.0	755	329	237	185	157	141	117	101
8	2.5119×10^8	8.4	755	345	249	197	169	153	129	113
9	6.3096×10^8	8.8	827	361	265	209	181	165	141	125
10	1.5849×10^9	9.2	827	377	277	221	193	177	153	137

Fig. 10 The area in the dashed blue box is chosen for illustrating the changes of boundary thickness

- For both $\mathrm{Re}=2.51\times10^6$ and $\mathrm{Re}=1.58\times10^9$, the maximum flow speed increases and boundary thickness decreases with the decrease of D/L;
- When $D/L=0.01$, where the distance between the flat plate and the parallel wall has the same order of magnitude as the boundary layer thickness, the boundary layer thickness decreases more significantly than that for $D/L\geq0.02$.

As a consequence, the velocity gradient normal to the flat plate increases leading to a rise of the local friction (C_{fx}). Figure 12 shows the results of C_{fx} at $Re=2.51\times10^6$ and $Re=1.58\times10^9$ in different shallow conditions.

Some remarks can be drawn from Fig. 12:

- For both Reynolds numbers, limited water depth has an increasing influence on C_{fx} from the leading edge to the trailing edge;
- The C_{fx} increases rapidly with the decrease of D/L;
- Influence of shallow water on local friction is more significant at the low Reynolds number. For example, at the trailing edge, when $D/L=0.01$, the increase of C_{fx} can be more than 50% at $Re=2.51\times10^6$ but is only 20% at $Re=1.58\times10^9$. This discrepancy shows important scale effects when extrapolating resistance in shallow water from model scale to full scale.

Consequently, the total frictional resistance, which is the sum of the local frictions, is also increased on shallow water conditions and depends on D/L as well.

4.2 The validity of zero-pressure gradient (ZPG) assumption

An assumption in the previous research [1–4, 11, 24] about the flow passing a flat plate is that the pressure gradient along the plate is zero. This makes it easier to derive theoretical solutions for friction lines and usually has a good agreement with experiments.

For an incompressible, two-dimensional laminar flow, the control equations within the boundary layer are

$$u\frac{\partial u}{\partial x}+v\frac{\partial u}{\partial y}=-\frac{1}{\rho}\frac{\partial p}{\partial x}+\frac{\partial^2 u}{\partial y^2}, \tag{2}$$

$$0=-\frac{\partial p}{\partial y},$$

$$\frac{\partial u}{\partial x}+\frac{\partial v}{\partial y}=0.$$

Blasius [25] (translated by NACA [26]) set the term $-\rho^{-1}\times\partial p/\partial x$ to zero in Eq. 2 and derived the Blasius solution.

For a two-dimensional, fully-developed turbulent flow, based on the ZPG assumption and a large amount of experiments results, Schlichting [19] fitted a formula for C_{f} in fully turbulent flow:

$$C_{\mathrm{f}}=\frac{0.455}{(\lg Re_x)^{2.58}}.$$

However, the validity of the ZPG in shallow water should be tested. In this study, two Reynolds numbers were again

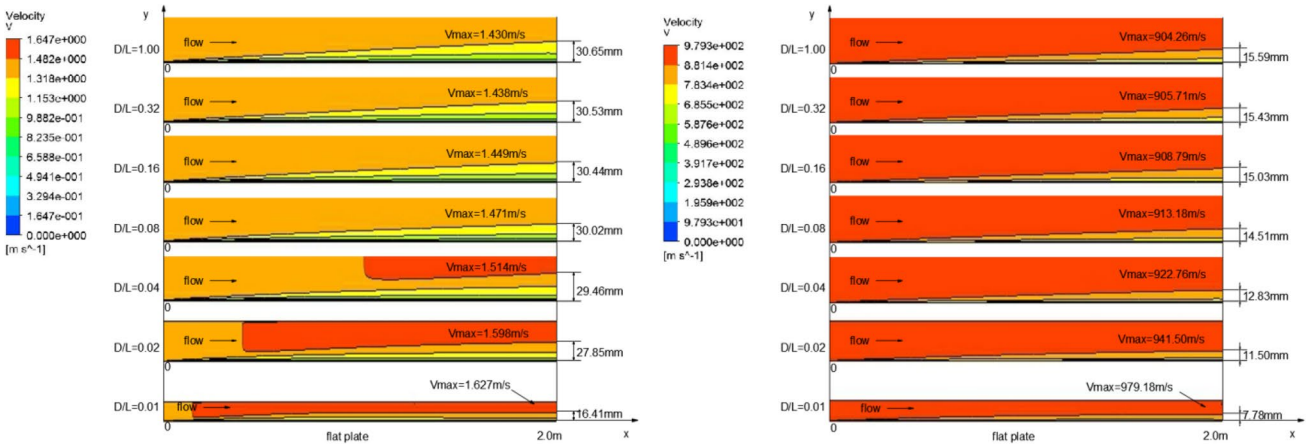

Fig. 11 The velocity contour close to the flat plate at different D/L (left: $Re=2.51\times10^6$, right: $Re=1.58\times10^9$; the boundary layer thickness ($0.99V_{\mathrm{max}}$) at $x=2$ m is shown at the right of the figure)

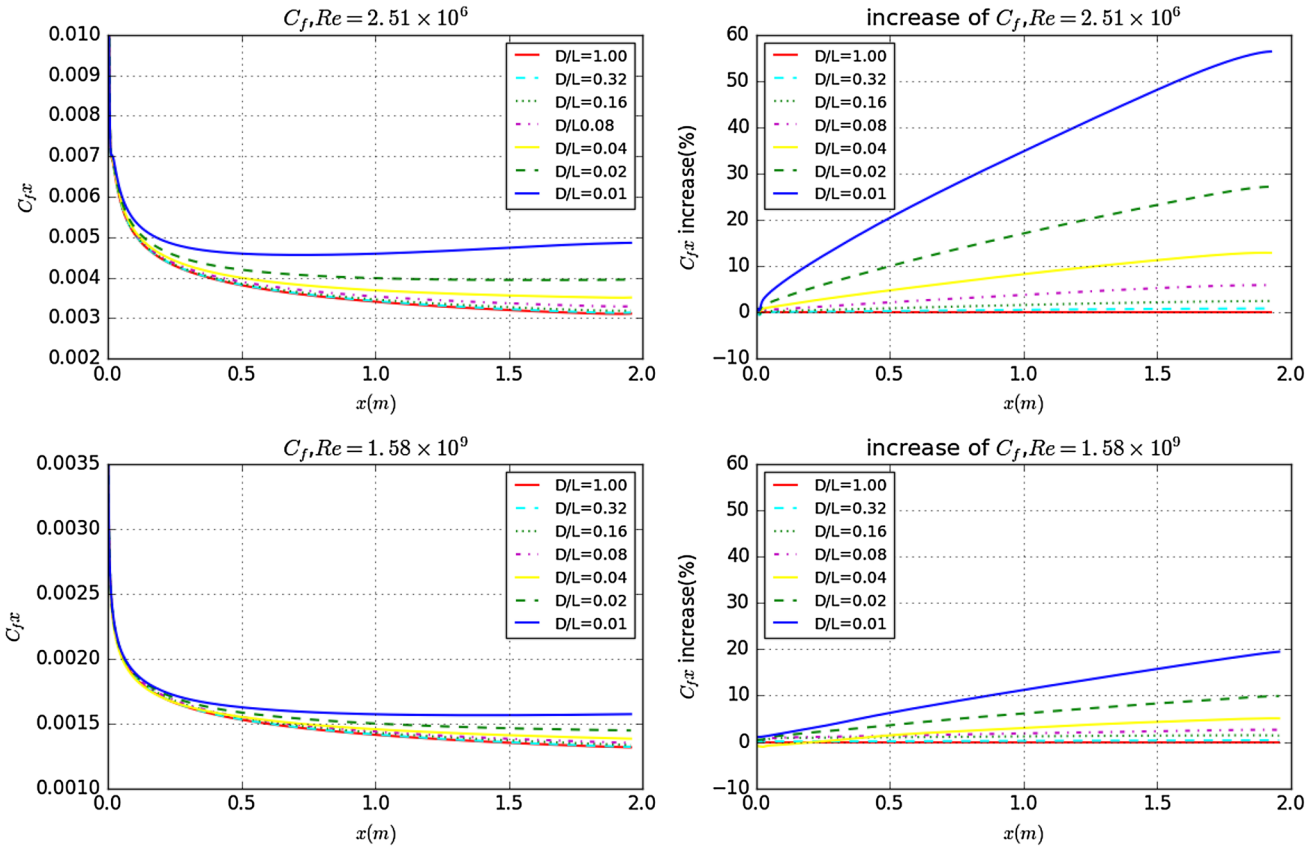

Fig. 12 Local friction resistance coefficient (C_{fx}) and C_{fx} increase compared to $D/L = 1.00$ (in percent) at in shallow water conditions

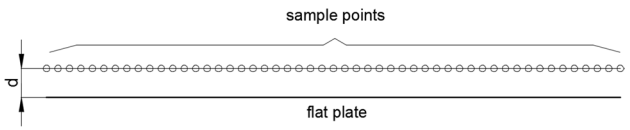

Fig. 13 Sample points near flat plate

chosen: $Re = 2.51 \times 10^6$ and $Re = 1.58 \times 10^9$. Sample points were picked on three straight lines which close to the boundary layer, with the same length of the flat plate and offset the plate by $d = 5$ mm, 10 mm, and 15 mm, as shown in Fig. 13. Values of pressure gradient and velocity gradient were recorded at these points.

To test the ZPG assumption, the problem becomes to compare the order of magnitude of $u\partial u/\partial x$ and $-\rho^{-1} \times \partial p/\partial x$. The ZPG assumption is valid only when they have the same order. Figure 14 presents the values of $u\partial u/\partial x$ and $-\rho^{-1} \times \partial p/\partial x$at different conditions.

When D/L is 1.00, $-\rho^{-1} \times \partial p/\partial x$are close to zero, which can be ignored compared to $u\partial u/\partial x$for both Reynolds numbers. However, when D/L drops to 0.01, the magnitude of $-\rho^{-1} \times \partial p/\partial x$increases significantly and even reaches the same order as $u\partial u/\partial x$.

Therefore, when D/L ratio is small enough, the item $-\rho^{-1} \times \partial p/\partial x$can no longer be ignored, both at low and high Reynolds numbers. In other words, the ZPG assumption is invalid at extremely shallow water conditions. Thus, those methods based on the zero-pressure gradient assumption are insufficient.

4.3 Shallow water effects on the frictional resistance

Results of the total frictional resistance coefficients of the flat plate and their increase compared with deep water condition (in percent) are presented in Fig. 15.

Based on Fig. 15, we can derive

- For relatively low Reynolds numbers, D/L significantly influences the C_f. For instance, when $\lg(Re) = 5.6$, the increase of C_f can reach almost 50% compared to the deep water condition;
- The influences from shallow water diminish with the increase of Reynolds number. For instance, when $\lg(Re) = 9.2$, the increase of C_f is only 10% compared to the deep water condition.

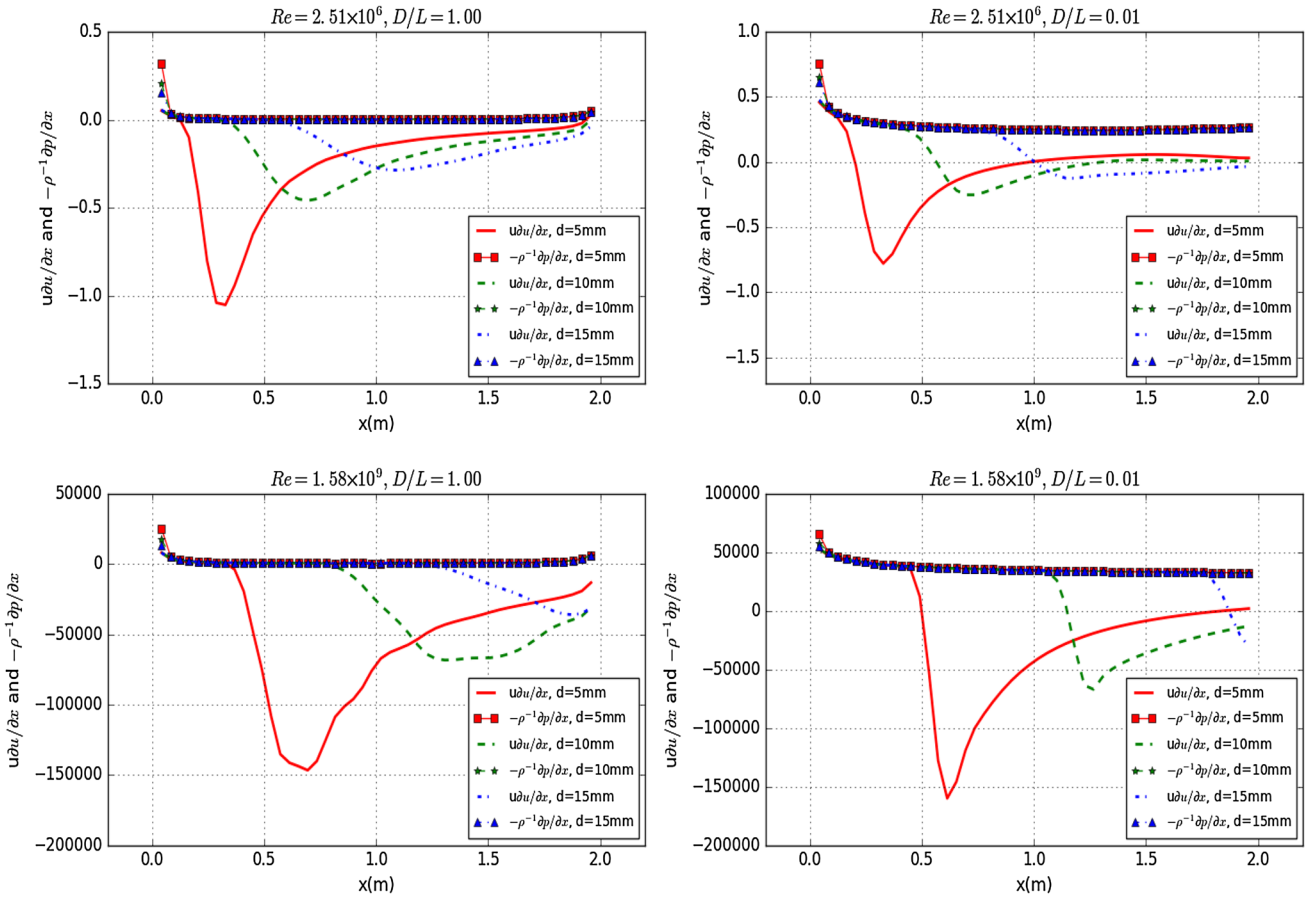

Fig. 14 Magnitude comparisons of $-\rho^{-1}\times\partial p/\partial x$ and $u\partial u/\partial x$ at four conditions (Case information is shown at the top of each sub-graph. The vertical axis denotes the magnitudes of $u\partial u/\partial x$ and$-\rho^{-1}\times\partial p/\partial x$. The horizontal axis shows the position from the leading edge to trailing edge of the flat plate)

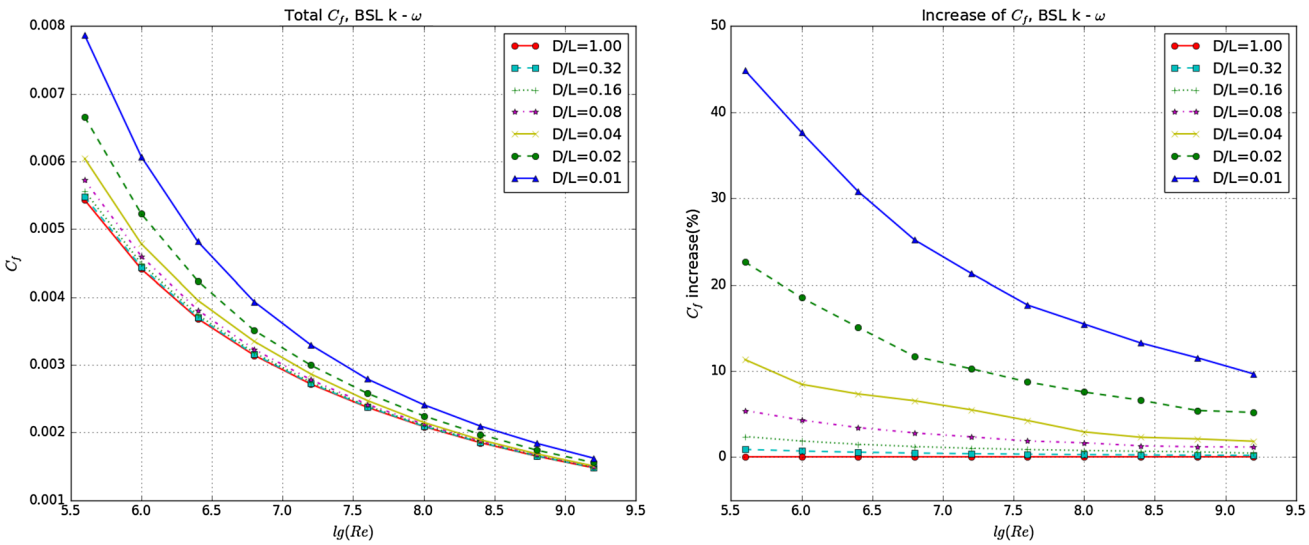

Fig. 15 Left: Total frictional resistance coefficient (C_f) with Reynolds number; Right: Increase of C_f compared with $D/L = 1.00$

As a result, the influence of shallow water conditions on the C_f again has scale effects, and the effect is larger at low *Re* because the boundary layer is thinner will is less likely to be influenced at high *Re*.

In practice, the scale effects at shallow water conditions may cause large errors in engineering. For instance, for an inland ship with 100 meters long and sails at 18 km/h (relative to the flow under the ship bottom), its Reynolds number is about 4.4×10^8, and it sails in shallow water with the $D/L=0.01$. When using a 1/25 scaled model, which has a Reynolds number about 3.5×10^6, to extrapolate the total resistance, C_f of the bottom part at full scale will increase by about 11% compared to deep water, but it will increase by about 28% at model scale according to this study. This discrepancy will lead to an unreliable resistance extrapolation if the IITC57 correlation line is applied. Consequently, a new friction line considering shallow water effect is needed to correct the shallow water effects.

4.4 The fitting of a numerical friction line

This section proposes a numerical friction line for correcting the shallow water effects on ship's bottom based on the described CFD calculations.

A regression analysis using the method of least squares was applied. During the procedure, choosing a suitable function model is essential to the quality of the fitting. Inspired by the ITTC57 [4] formula, we chose the function model as follows:

$$C_f=\frac{a}{(\lg Re-b)^c}$$

The *a, b* and *c* are constants defined in the fitting. In this study, we followed two steps in the regression analysis: first, fit a numerical friction line in deep water condition using the results of $D/L=1.00$; Second, include the parameter D/L based on the numerical results of other values of D/L.

The result for the first fitting with the *R*-squared value (a statistical measure of how close the data are to the fitted regression line) of 0.9996 is shown as follows:

$$C_{f\_deep}=\frac{0.08169}{(lgRe-1.717)^2} \tag{3}$$

The C_f in shallow water conditions depends on Reynolds number and D/L, and additionally, when D/L is close to 1, which approaches the deep water, the numerical friction line should approach the Eq. 3.

Based on the results of the simulations, a numerical friction line in shallow water conditions is proposed using regression analysis:

$$C_{f\_proposed}=\frac{0.08169}{(lgRe-1.717)^2}\times\left(1+\frac{0.003998}{lgRe-4.393}\cdot\left(\frac{D}{L}\right)^{-1.083}\right).$$

Re is Reynolds number; *D* is the distance between flat plate and parallel wall; *L* is the length of the flat plate.

Errors between the simulations and the new proposed friction line are shown in Table 11.

The errors are mostly less than 1%, except when $D/L=0.01$(still less than 3%). This error table can be referred when using this new friction line.

4.5 Application and a case study

The previous section proposed a modification of the ITTC57 correlation line. However, since a ship also has non-horizontal wetted surfaces, this method cannot be applied directly. In this paper, it is suggested to modify the frictional resistance on the flat bottom area with the proposed friction line and apply the ITTC57 correlation line for the non-horizontal wetted surface. Therefore, we propose the following steps to use this method in the prediction of the frictional resistance of an actual ship:

Table 11 Errors between simulations and the proposed friction line

Re	*D/L*						
	1.00	0.32	0.16	0.08	0.04	0.02	0.01
3.9811×10^5	0.11%	0.03%	−0.18%	−0.50%	−0.66%	0.04%	2.33%
1.0000×10^6	1.19%	1.10%	0.89%	0.51%	0.64%	−0.16%	0.07%
2.5119×10^6	1.35%	1.28%	1.11%	0.81%	0.37%	0.03%	−0.10%
6.3096×10^6	0.85%	0.79%	0.67%	0.45%	−0.37%	0.50%	0.01%
1.5849×10^7	0.20%	0.16%	0.08%	−0.08%	−0.73%	−0.30%	−0.30%
3.9811×10^7	−0.35%	−0.38%	−0.45%	−0.42%	−0.65%	−0.57%	0.05%
1.0000×10^8	−0.74%	−0.75%	−0.80%	−0.80%	−0.17%	−0.74%	−0.16%
2.5119×10^8	−1.00%	−1.00%	−1.04%	−0.87%	−0.17%	−0.82%	0.10%
6.3096×10^8	−1.16%	−1.15%	−1.19%	−1.04%	−0.42%	−0.43%	0.31%
1.5849×10^9	−1.24%	−1.23%	−1.16%	−1.20%	−0.46%	−0.78%	0.96%

a. Use the ship's physical or digital model to obtain the area of the total wetted surface (S_T) and the area of flat bottom (S_B);
b. Calculate the Reynolds number ($Re_{\_0}$) of the incoming flow with the free stream velocity ($V_{\_0}$);
c. Calculate the Reynolds number ($Re_{\_B}$) of the water underneath ship's bottom with the incoming velocity ($V_{\_B}$) derived from CFD calculations by averaging the velocity at the leading edge of the flat bottom;
d. Apply the ITTC57 correlation line to calculate the conventional frictional resistance coefficient C_{f_0};
e. Use the proposed friction line to calculate the coefficient ($C_{f\_proposed}$) in shallow water, and use the Katsui's line to calculate the friction coefficient (C_{f_Katsui}) of flat plate in unrestricted conditions;
f. The corrected total frictional resistance coefficient (C_f) of ship in shallow water can be predicted as

$$C_f = C_{f\_0} + \left(C_{f\_proposed} - C_{f\_Katsui}\right) \times \left(\frac{S_B}{S_T}\right) \times \left(\frac{V_{\_B}}{V_{\_0}}\right)^2. \tag{4}$$

It should be pointed out that the Katsui's line used in Eq. 4 can be replaced by any other suitable deep water friction line.

As a case study, the above steps are applied for a 1/30 scaled model ship, whose prototype is an 86-m long inland ship. The free surface is not considered in CFD calculations to eliminate wave effects on friction. Details of the ship parameters can be found in [10]. L here is the length of the flat bottom.

To achieve the average velocity ($V_{\_B}$) at the leading edge of the wide flat bottom (as indicated in Fig. 3), a systematic CFD calculation has been done for various incoming velocities and water depths. The results of $V_{\_B}$ are shown in Fig. 16, and an empirical formula is regressed for this specific case with an uncertainty of 2.5%:

For $h/T \le 4.0$,

$$V_{\_B} \equiv V + \Delta V = 0.4277 \times V \times \exp\left\{\left(\frac{h}{T}\right)^{-0.07634}\right\}.$$

Following the steps shown at the beginning of this section, the frictional resistance of this ship model is predicted at 0.8 and 1.0 m/s in various water depths, as shown in Table 12.

For all the three different water depths, results of C_f using the proposed method agrees better with the values derived from CFD than ITTC57. With the errors less than 3%, the improved correlation line is practically considered applicable to successfully predict the friction including shallow water effects on ship's flat bottom.

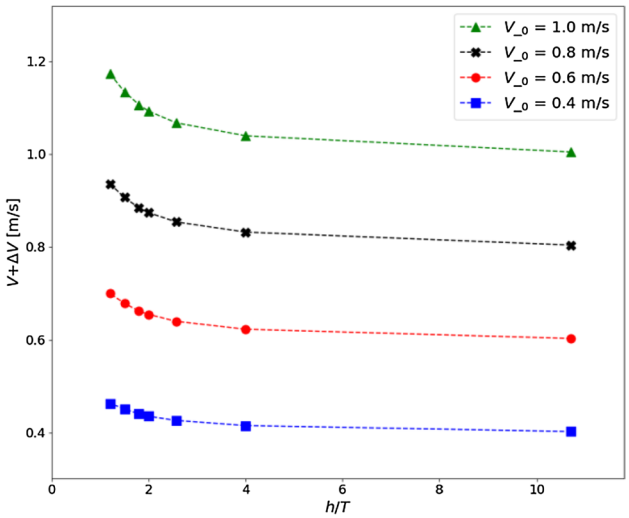

Fig. 16 The average velocity at the leading edge of the flat bottom against water depth

5 Conclusions

This study has proposed a numerical friction line for correcting shallow water effects on ship's bottom on shallow water conditions using CFD calculations.

A moving plate approaching a flat plate was applied to build the shallow water conditions. Three fully turbulence models (Spalart–Allmaras, BSL k-ω, and SST k-ω) and one transition model (k-kl-ω) were applied to verify and validate the numerical calculations. Practically, the BSL k-ω was the most suitable model, and the turbulence intensity of 6% with the turbulent viscosity ratio of 100 was the best inlet boundary condition in this study.

Based on the calculations in shallow water conditions, we concluded

- For low Reynolds numbers, D/L significantly influences the friction on the flat plate. When $\lg(Re) = 5.6$, the increase of C_f can reach almost 50% compared to the deep water condition;
- The influence of shallow water on friction has scale effects, which diminishes with the increase of Reynolds number. For a relatively high Reynolds number (e.g. $\lg(Re) = 9.2$), the increase of C_f is only 10% compared to the deep water condition;
- The zero-pressure gradient assumption is invalid in extremely shallow water.

Reynolds number is no longer the only factor influencing friction at shallow water conditions. A numerical friction line considering the shallow water effects and the scale effects is proposed. After applying this proposed line to modify the frictional resistance on ship's bottom can

Table 12 An example of applying the proposed friction line

$V_{\_0}$ (m/s)	$V_{\_B}$ (m/s)	h/T	D/L	C_f from CFD	ITTC57		Proposed method	
					C_f	Error (%)	C_f	Error (%)
0.8	0.800	10.71	0.3952	3.886×10^{-3}	4.049×10^{-3}	4.19	4.049×10^{-3}	4.19
	0.882	2.01	0.0411	4.187×10^{-3}	4.049×10^{-3}	−3.29	4.133×10^{-3}	−1.28
	0.916	1.20	0.0081	4.555×10^{-3}	4.049×10^{-3}	−11.11	4.540×10^{-3}	−0.33
1	1.000	10.71	0.3952	3.760×10^{-3}	3.872×10^{-3}	3.00	3.872×10^{-3}	3.00
	1.102	2.01	0.0411	4.058×10^{-3}	3.872×10^{-3}	−4.58	3.961×10^{-3}	−2.40
	1.145	1.20	0.0081	4.421×10^{-3}	3.872×10^{-3}	−12.41	4.390×10^{-3}	−0.69

combine the ITTC57 correlation line for other wetted surface, ship's frictional resistance in pure shallow water can be better predicted.

For resistance extrapolation in shallow water from ship models to full-scale ships, the proposed friction line can also correct the scale effect on the friction on ship's bottom and thus, increase the reliability of the model-ship extrapolation of resistance.

In the future, more factors will be considered to improve the prediction of ship's frictional resistance in shallow water. Ship waves, trim and sinkage are all possible factors influencing ship friction. The physical explanation proposed in this paper, which shows the changes in the boundary layer, is applicable if those factors are considered in the future research. The modification to include the parameters of the waterway also shows the way to update the friction or model-ship correlation line in shallow water.

Acknowledgements This research is funded by the China Scholarship Council (CSC).

References

1. Schoenherr KE (1932) On the resistance of flat surfaces moving through a fluid. Trans SNAME 40:279
2. Grigson C (1999) A planar friction algorithm and its use in analysing hull resistance. Trans RINA 142:76–115
3. Katsui T, Asai H, Himeno Y, Tahara Y (2005) The proposal of a new friction line. In: Fifth Osaka colloquium on advanced CFD applications to ship flow and hull form design, Osaka, Japan
4. ITTC (1957) In 8th International Towing Tank Conference, Madrid, Spanish
5. ITTC (1987) Report of the resistance and flow committee. In: 18th international towing tank conference, Kobe, Japan
6. Schlichting O (1934) Ship resistance in water of limited depth-resistance of sea-going vessels in shallow water (trans: Roemer MC, 1940). Jahrbuch der STG 35:127–148
7. Lackenby H (1963) The effect of shallow water on ship speed. Shipbuilder Marine Eng 70:446–450
8. Jiang T (2001) A new method for resistance and propulsion prediction of ship performance in shallow water. In: Proceedings of the 8th international symposium on practical design of ships and other floating structures, Shanghai, China
9. Linde F et al (2016) Three-dimensional numerical simulation of ship resistance in restricted waterways: effect of ship sinkage and channel restriction. J Waterway Port Coast Ocean Eng 143:06016003
10. Zeng Q et al (2017) Numerical and experimental study of resistance, trim and sinkage of an inland ship model in extremely shallow water. In: International conference on computer applications in shipbuilding (ICCAS2017). RINA, Singapore. pp. 19–25
11. Eça L, Hoekstra M (2008) The numerical friction line. J Marine Sci Technol 13(4):328–345
12. Eloot K, Vantorre M (2011) Ship behaviour in shallow and confined water: an overview of hydrodynamic effects through efd. In: Specialists' meeting on assessment of stability and control prediction methods for air and sea vehicles (AVT-189/RSM-028), Portsdown, United Kingdom
13. Ansys IC (2015) 16.2 Help Manual. Ansys Inc
14. ANSYS (2017) ANSYS® Academic Research, Release 18.1, Help System, Fluent User's Guide. Ansys Inc
15. Walters DK, Cokljat D (2008) A three-equation eddy-viscosity model for Reynolds-averaged Navier–Stokes simulations of transitional flow. J Fluids Eng 130(12):121401
16. Roache PJ (1998) Verification and validation in computational science and engineering. Hermosa, Albuquerque
17. Eça L, Hoekstra M (2009) Evaluation of numerical error estimation based on grid refinement studies with the method of the manufactured solutions. Comput Fluids 38(8):1580–1591
18. Eça L, Hoekstra M (2014) A procedure for the estimation of the numerical uncertainty of CFD calculations based on grid refinement studies. J Comput Phys 262:104–130
19. Schlichting H (1941) /42) Lecture series: Boundary layer theory (translated by NACA technical memorandum No. 1218). Luftfahrtforschungsanstalt Hermann Gooring, Braunschweig
20. Nagib HM, Chauhan KA, Monkewitz PA (2007) Approach to an asymptotic state for zero pressure gradient turbulent boundary layers. Philos Trans R Soc Lond A Math Phys Eng Sci 365(1852):755–770
21. Hughes G, Allan J (1951) Turbulence stimulation on ship models. SNAME Trans 59:281–314
22. Nagib HM, Christophorou C, Monkewitz PA High Reynolds number turbulent boundary layers subjected to various pressure-gradient conditions. In: IUTAM symposium on one hundred Years of boundary layer research. Springer
23. Österlund JM (1999) Experimental studies of zero pressure-gradient turbulent boundary layer flow. Royal Institute of Technology, Stockholm, Sweden

24. Todd F (1951) Skin friction resistance and the effects of surface roughness. SNAME Trans 59:315–374
25. Blasius H (1908) Grenzschichten in Flüssigkeiten mit kleiner Reibung. Zeitschrift fur Mathematik Physik 56:1–37
26. NACA (1950) English translation of Blasius' original paper. NACA Technical Memorandum 1256